

Electronic supplementary information

Siloxane-decorated polymer acceptors enable humidity-tolerant air-processing and mechanical durability of all-polymer solar cells

Peng Dou,^{a,‡} Qingqing Bai,^{a,‡} Xinkang Wang,^{a,‡} Mei Luo,^a Jialong Xie,^a Jong Bin Park,^c Junyi Lu,^b Henan Li,^b Qian Liu,^b Siyu Zhao,^a Han Young Woo,^c Huiliang Sun,^{*b} Lianjie Zhang^{*a} and Junwu Chen^{*a}

^a Institute of Polymer Optoelectronic Materials & Devices, Guangdong Basic Research Center of Excellence for Energy & Information Polymer Materials, State Key Laboratory of Luminescent Materials & Devices, South China University of Technology, Guangzhou 510640, China. E-mail: lianjiezhang@scut.edu.cn; psjwchen@scut.edu.cn

^b Center for Advanced Analytical Science, Guangzhou Key Laboratory of Sensing Materials and Devices, Guangdong Engineering Technology Research Center for Photoelectric Sensing Materials and Devices, School of Chemistry and Chemical Engineering, Guangzhou University, Guangdong 510006, China. E-mail: huiliang@gzhu.edu.cn

^c Department of Chemistry, College of Science, KU-KIST Graduate School of Converging Science and Technology, Korea University, Seoul 136-713, Republic of Korea

‡ These authors contributed equally to this article.

Experimental Section

UV-vis absorption spectra

UV-vis absorption spectra were recorded on an HP 8453 spectrophotometer.

Energy level measurement of cyclic voltammetry (CV)

CV was performed with a CHI660A electrochemical work station. All measurements were carried out in a one-compartment cell under a nitrogen atmosphere, equipped with a glassy-carbon electrode, a platinum counter-electrode, and an Ag/Ag⁺ reference electrode with a scan rate of 50 mV/s. The supporting electrolyte was a 0.1 mol/L acetonitrile solution of tetrabutylammonium hexafluorophosphate (Bu₄NPF₆). All potentials were referenced to the ferrocenium/ferrocenecouple (Fc/Fc⁺) by using ferrocene as an internal standard. The deposition of a copolymer on the electrode was done by the evaporation of a dilute chloroform solution.

Device fabrication of the all-polymer solar cells (all-PSCs)

The conventional structure of glass/ITO/PEDOT:PSS/active layer/PDNIT-F3N/Ag was used for all-PSC devices. The pre-patterned ITO-coated glass substrates were cleaned by sequential sonication in deionized water, acetone, and isopropanol for 15 min, respectively, followed by UV-ozone treatment for 15 min. PEDOT:PSS was spin-coated onto the UV-ozone-treated ITO substrates at 3500 rpm for 30 s and then annealed at 150 °C for 15 min to form a ~35 nm film. For devices fabricated in a nitrogen environment, the PEDOT:PSS-coated ITO substrates were transferred into an N₂-filled glovebox, where the active layer (PM6:DSiX blend, 1:1 weight ratio in *o*-xylene with 2% 1-chloronaphthalene additive) was spin-coated at 3000 rpm for 40 s (20 mg mL⁻¹). For air-processed devices, the active layer was deposited directly in ambient air under controlled humidity (65% or 90%, adjusted via a humidifier and monitored with a hygrometer). The PDNIT-F3N was dissolved in methanol at the concentration of 1.0 mg mL⁻¹ and spin-coated at 3000 rpm for 30 s on the active layer. 110 nm Ag was sequentially deposited onto the top of the active layer in an evaporation chamber under a high vacuum with an area of 4.5 mm². All current-voltage (*J-V*) characteristics of the devices were measured under simulated AM1.5G irradiation (100 mW cm⁻²) using an

Xe lamp-based SS-F5-3A Solar Simulator (Enli Technology, Inc.). An Xe lamp equipped with an AM1.5G filter was used as the white light source. The light intensity was controlled with an NREL-calibrated Si solar cell with a KG-5 filter. The external quantum efficiency (EQE) was measured by a QE-R3011 measurement system (Enli Technology, Inc.).

Space-charge-limited current (SCLC) measurements.

The electron-only devices were fabricated with ITO/ZnO/Active layer/PNDIT-F3N/Ag structures and hole-only devices were fabricated with ITO/PEDOT:PSS/Active layer/MoOx/Ag structures. The SCLC mobility was calculated according to the Mott-Gurney square law:

$$J = \frac{9}{8} \varepsilon_0 \varepsilon_r \mu \frac{V^2}{L^3}$$

where J is the current density, ε_r is the relative dielectric constant of the transport medium component, ε_0 is the vacuum permittivity, μ is the electron or hole mobility, V is the effective voltage, and L is the thickness of active layer.

Contact angle measurement

The surface tension was measured through pending drop technique on a drop shape analyzer (Betop Scientific DSA-XPlus) at room temperature. The surface energy values were calculated according to Wu model. Flory-Huggins interaction parameter, χ of the four binary combinations from contact angle measurements using the formula ($\chi_{D,A} \propto (\sqrt{\gamma_D} - \sqrt{\gamma_A})^2$), where D and A are the individual components in blends.

Atomic force microscopy-based infrared spectroscopy (tapping AFM-IR)

AFM-IR was performed by Anasys nanoIR3 (Bruker).

J_{SC} and V_{OC} on the light intensity (P_{light}) dependence

The correlation between J_{SC} and light intensity (P_{in}) can be expressed as $J_{SC} \propto P_{light}^\alpha$, where α is close to 1 suggesting minimal bimolecular recombination. The dependence of V_{OC} on light intensity is examined to further understand the recombination processes. Generally, with a slope s close to $k_B T/q$ (where k_B is the

Boltzmann constant, T is the temperature in Kelvin, q is the elementary charge), trap-assisted recombination should be negligible.

$$V_{OC} \propto \frac{\alpha k_B T}{q} \ln(P_{light})$$

Photoluminescence (PL) and time-resolved photoluminescence (TRPL)

PL spectra of thin films were recorded using a Horiba Fluoromax-4 spectrofluorometer. TRPL was performed using Horiba Fluorolog-3 Time-Correlated Single Photon Counting system. The PM6:DSiX, and PM6:PY-IT blends were excited by 450 nm laser and detected at its PL emission peak 669 nm.

Transmission electron microscopy (TEM)

TEM images were acquired using JEM-2100F Field Emission Electron Microscope with an accelerating voltage of 30 kV.

XPS measurement

X-ray photoelectron spectroscopy (XPS) was determined by British Kratos X-ray photoelectron spectroscopy for element analysis.

Grazing incidence wide angle scattering (GIWAXS)

GIWAXS measurement was carried out with a Xeuss 2.0 SAXS/WAXS laboratory beamline using a Cu X-ray source (8.05 keV, 1.54 Å) and a Pilatus3R 300K detector. The incidence angle is 0.2°. The samples for GIWAXS measurements are fabricated on silicon substrates using the same recipe for the devices.

Fourier transform infrared spectrometer (FTIR microscope)

Nicolet IS50 - Nicolet Continuum

Maximum power point tracking (MPPT) measurements

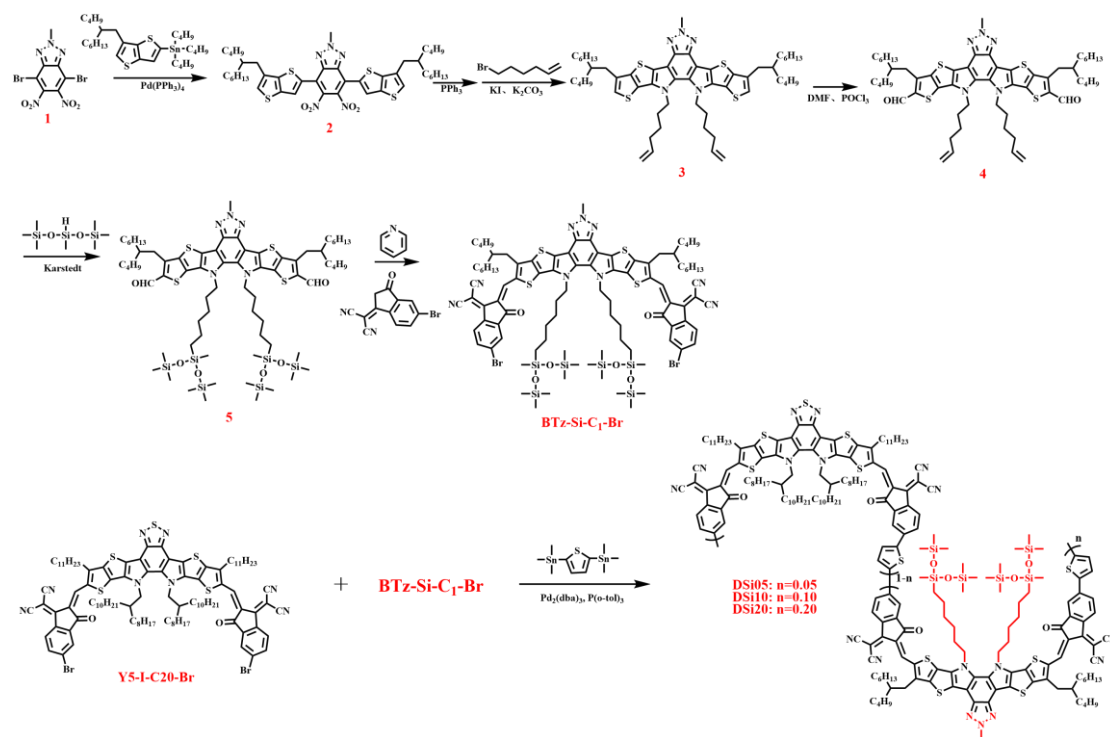
The device photostability was measured using the solar cell stability system (PR-SCCS-C5T3Q, Shenzhen PURI, China) in an N₂ atmosphere, which was conducted under continuous 100 mW cm⁻² illumination provided by a white LED, and the results were automatically recorded by the aging test software.

Materials and synthesis

All reagents and solvents were purchased from Aldrich, J&K Co., Aladdin Co., Innochem Co., Acros, SunaTech Co. and other commercial suppliers. 2,5-

Bis(trimethylstannyl)thiophene (T-2Sn) and 2,2'-((2Z,2'Z)-((12,13-bis(2-octyldodecyl)-3,9-diundecyl-12,13-dihydro-[1,2,5]thiadiazolo[3,4-e]thieno[2'',3'':4',5']thieno[2',3':4,5]pyrrolo[3,2-g]thieno[2',3':4,5]thieno[3,2-b]indole-2,10-diyl)bis(methaneylyliden e))bis(5-bromo-3-oxo-2,3-dihydro-1H-indene-2,1-diylidene))dimalononitrile (Y5-I-C20-Br) were purchased from Volt-Amp Optoelectronics. All manipulations involving air-sensitive reagents were performed under an atmosphere of dry argon.

^1H and ^{13}C spectra were measured with Bruker AV 500 spectrometers. Chemical shifts for hydrogens are reported in parts per million (ppm, scale) downfield from tetramethylsilane and are referenced to the residual protons in the NMR solvent (CDCl_3 : 7.26). ^{13}C NMR spectra were recorded at 125 MHz. Chemical shifts for carbons are reported in parts per million (ppm, scale) downfield from tetramethylsilane and are referenced to the carbon resonance of the solvent (CDCl_3 : 77.16). The data are presented as follows: chemical shift, multiplicity (s = singlet, d = doublet, t = triplet, m = multiplet and/or multiple resonances), coupling constant in hertz (Hz), and integration.



Scheme S1. The synthetic routes of DSi-series polymer acceptors.

Compound **1** was synthesized in our lab according to the procedures reported in the

literature,¹ and the detailed synthesis processes of the monomers and polymers are described in the following.

Synthesis of 4,7-bis(6-(2-butyloctyl)thieno[3,2-b]thiophen-2-yl)-2-methyl-5,6-dihydro-2H-benzo[d][1,2,3]triazole (2)

Under argon atmosphere, **compound 1** (4.6 g, 12 mmol) and tributyl(6-(2-butyloctyl)thieno[3,2-b]thiophen-2-yl)stannane (18 g, 30 mmol) were added to a 250 mL two-neck round-bottom flask, followed by anhydrous *o*-xylene (150 mL) to dissolve the solids. The solution was stirred for 15 min before adding Pd(PPh₃)₄ (0.4 mmol, 0.5 g). The reaction mixture was then heated and refluxed to 120 °C and maintained at this temperature for 24 h. After reaction completed, the mixture was cooled to room temperature, and the solvent was removed by rotary evaporation to yield the crude product. Purification was performed by silica gel column chromatography using a petroleum ether/dichloromethane (4:1) mixture as the eluent, affording **compound 2** as red solid (yield: 49%). ¹H NMR (500 MHz, chloroform-*d*) δ 7.73 (s, 2H), 7.12 (s, 2H), 4.65 (s, 3H), 2.69 (d, *J* = 7.1 Hz, 4H), 1.86 (s, 2H), 1.35 – 1.25 (m, 32H), 0.88 (dt, *J* = 10.4, 6.7 Hz, 12H)

Synthesis of 3,9-bis(2-butyloctyl)-12,13-di(hex-5-en-1-yl)-6-methyl-12,13-dihydro-6H-thieno[2'',3'':4',5']thieno[2',3':4,5]pyrrolo[3,2-g]thieno[2',3':4,5]thieno[3,2-b][1,2,3]triazolo[4,5-e]indole (3)

Under argon atmosphere, **compound 2** (5 g, 6 mmol) and PPh₃ (15.7 g, 60 mmol) were added to a 250 mL two-neck round-bottom flask, followed by *N*-methylpyrrolidone (NMP, 150 mL) to fully dissolve the solid mixture. The solution was stirred while gradually increasing the reaction temperature to 180 °C and maintained overnight. When the reaction finished, heating was stopped, and the mixture was allowed to cool to room temperature. K₂CO₃ (3.43 g, 60 mmol), KI (0.43 g, 2.4 mmol), and 2-ethylhexyl bromide (9.0 g, 29.4 mmol) were then added sequentially. The mixture was stirred thoroughly before heating to 90 °C and held overnight. After the reaction finished, heating was stopped, and the mixture was cooled to room temperature. The

reaction mixture was then poured into 90 mL of ammonium chloride solution and extracted multiple times with small portions of dichloromethane (DCM). The combined organic layers were concentrated under reduced pressure to remove the solvent, yielding the crude product. Purification was carried out by silica gel column chromatography using a petroleum ether/dichloromethane (6:1) mixture as the eluent, affording **compound 3** as red-orange solid (yield: 35%). ¹H NMR (500 MHz, chloroform-*d*) δ 6.96 (s, 2H), 5.60 (ddt, *J* = 17.1, 10.4, 6.7 Hz, 2H), 4.87 – 4.79 (m, 4H), 4.63 (s, 3H), 4.60 (d, *J* = 7.8 Hz, 4H), 2.74 (d, *J* = 7.3 Hz, 4H), 2.04 – 1.96 (m, 2H), 1.92 (q, *J* = 7.2 Hz, 4H), 1.78 (p, *J* = 7.7 Hz, 4H), 1.38 – 1.24 (m, 32H), 1.19 (t, *J* = 7.7 Hz, 4H), 0.89 (q, *J* = 7.2 Hz, 12H).

Synthesis of 3,9-bis(2-butyloctyl)-12,13-di(hex-5-en-1-yl)-6-methyl-12,13-dihydro-6H-thieno[2'',3''':4',5']thieno[2',3':4,5]pyrrolo[3,2-g]thieno[2',3':4,5]thieno[3,2-b][1,2,3]triazolo[4,5-e]indole-2,10-dicarbaldehyde (4)

Under argon atmosphere, **compound 3** (1.32 g, 1.41 mmol) was dissolved in dimethylformamide (DMF, 20 mL) and transferred to a 250 mL two-neck round-bottom flask. While maintaining an ice-water bath, POCl₃ (2.1 mL, 22.05 mmol) was added slowly. The reaction mixture was stirred for 2 h before raising the temperature to 90 °C and kept at 90 °C overnight. After heating was stopped, the reaction mixture was poured into 100 mL of ice water and neutralized with a saturated sodium hydroxide solution. The organic compounds were extracted multiple times with small portions of DCM. The combined organic layers were concentrated under reduced pressure to remove the solvent. Finally, the crude product was purified by column chromatography (petroleum ether: dichloromethane = 1: 1), affording **compound 4** as yellow solid (yield: 80%). ¹H NMR (500 MHz, chloroform-*d*) δ 10.11 (s, 2H), 5.62 – 5.53 (m, 2H), 4.87 – 4.79 (m, 4H), 4.66 (d, *J* = 7.8 Hz, 3H), 4.64 (s, 4H), 3.10 (d, *J* = 7.5 Hz, 4H), 2.06 (d, *J* = 12.2 Hz, 2H), 1.92 (q, *J* = 7.2 Hz, 4H), 1.78 (p, *J* = 8.0 Hz, 4H), 1.37 – 1.28 (m, 32H), 1.20 (d, *J* = 7.6 Hz, 4H), 0.88 (dd, *J* = 7.2, 2.5 Hz, 12H).

Synthesis of 3,9-bis(2-butyloctyl)-12,13-bis(6-(1,1,1,3,5,5,5-heptamethyltrisiloxan-3-yl)hexyl)-6-methyl-12,13-dihydro-6H-thieno[2'',3''':4',5']thieno[2',3':4,5]pyrrolo[3,2-g]thieno[2',3':4,5]thieno[3,2-b][1,2,3]triazolo[4,5-e]indole-2,10-dicarbalde

hyde (5)

Under argon atmosphere, **compound 4** (1 g, 1 mmol) and bis(trimethylsiloxy)methylsilane (6 mmol) were added to a 250 mL two-neck round-bottom flask and dissolved in anhydrous tetrahydrofuran (THF) under light protection. Karstedt catalyst (0.1 mL) was added dropwise to the reaction mixture, which was then heated to 65°C and stirred overnight. The reaction was quenched by pouring the mixture into ice water, followed by multiple extractions with small portions of DCM. The combined organic layers were concentrated using a rotary evaporator to remove the solvent. The crude product was purified by silica gel column chromatography using a petroleum ether/ethyl acetate (20:1) mixture as the eluent, affording **compound 5** as pale yellow solid (yield: 45%). ¹H NMR (500 MHz, chloroform-*d*) δ 10.09 (s, 2H), 4.62 (s, 4H), 3.09 (d, *J* = 7.5 Hz, 4H), 2.06 (s, 2H), 1.74 (s, 4H), 1.36 (s, 12H), 1.31 – 1.10 (m, 28H), 0.86 (q, *J* = 7.2 Hz, 10H), 0.28 (d, *J* = 9.3 Hz, 4H), -0.01 (s, 36H), -0.11 (s, 6H).

Synthesis of BTz-Si-C₁-Br

Under argon atmosphere, **compound 5** (0.5 g, 0.35 mmol) and IC-Br (2.13 mmol) were added to a 100 mL two-neck round-bottom flask, followed by chloroform (50 mL) to fully dissolve the solids. After stirring, pyridine (2 mL) was added, and the reaction mixture was heated to reflux at 75 °C for 8 h. The reaction was then stopped, and the crude product was purified by silica gel column chromatography, affording **BTz-C₁-Si-Br** (yield: 85%). ¹H NMR (500 MHz, chloroform-*d*) δ 8.73 (s, 2H), 8.44 (d, *J* = 8.3 Hz, 2H), 7.89 (s, 2H), 7.68 (d, *J* = 8.2 Hz, 2H), 4.73 (s, 3H), 4.70 (s, 4H), 3.01 (s, 4H), 2.01 (s, 2H), 1.94 (s, 4H), 1.39 (s, 12H), 1.27 (d, *J* = 24.5 Hz, 28H), 0.85 (dt, *J* = 18.7, 6.8 Hz, 10H), 0.39 (t, *J* = 8.1 Hz, 4H), -0.01 (d, *J* = 3.2 Hz, 36H), -0.08 (s, 6H). ¹³C NMR (101 MHz, chloroform-*d*) δ 136.09, 135.86, 126.98, 124.01, 113.54, 49.48, 41.50, 37.79, 32.83, 31.61, 31.37, 31.15, 29.98, 29.72, 27.82, 27.00, 24.82, 24.76, 21.20, 21.18, 20.79, 15.74, 12.23, -1.89, -2.06.

Synthesis of DSiX

DSi05: Under argon atmosphere, Y5-I-C20-Br (0.15 mmol), T-2Sn (0.16 mmol), Pd₂(dba)₃ (4.5 mg), P(*o*-Tol)₃, and **BTz-Si-C₁-Br** (0.0075 mmol) were added to a 25

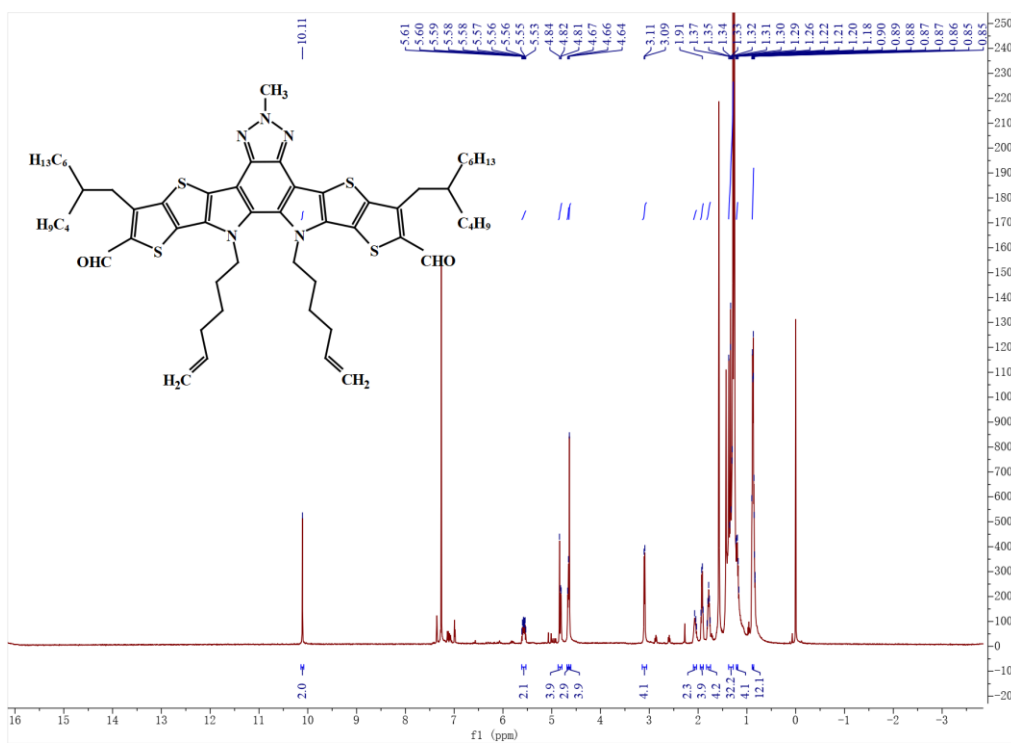
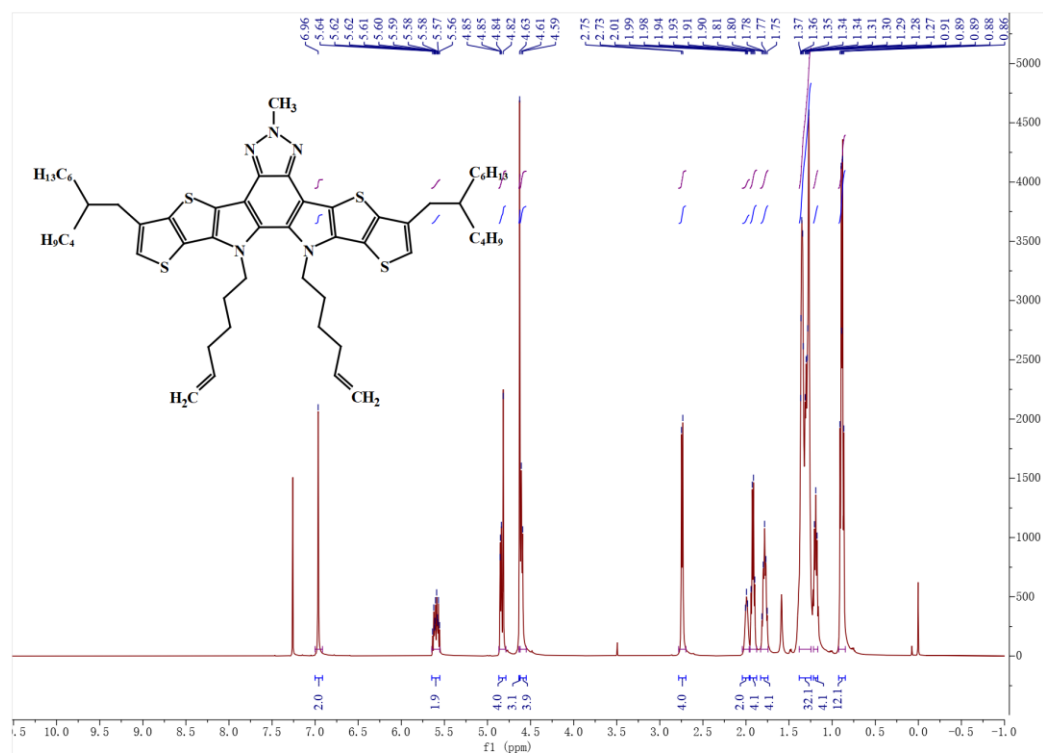
mL two-neck round-bottom flask, followed by anhydrous *o*-xylene (5 mL) to fully dissolve the solids. The reaction mixture was heated to 120 °C and stirred for three days. After reaction was finished, the reaction mixture was slowly added into 100 mL of anhydrous methanol to precipitate the product. The precipitate was collected by filtration and further purified by Soxhlet extraction, sequentially using methanol, ethanol, acetone, ethyl acetate, petroleum ether, and dichloromethane. The dichloromethane fraction was collected and concentrated and then added dropwise into 150 mL of methanol to induce precipitation, yielding **DSi05** as a black solid (84% yield). High-temperature GPC analysis GPC: $M_n=9.1 \text{ kg mol}^{-1}$, $M_w=17.37 \text{ kg mol}^{-1}$, PDI=1.89.

The synthetic procedures for **DSi10** and **DSi20** were similar to that of **DSi05**, with yields of approximately 85%.

High-temperature GPC analysis of **DSi10**: $M_n = 8.7 \text{ kg mol}^{-1}$, $M_w = 16.90 \text{ kg mol}^{-1}$, PDI = 1.93.

High-temperature GPC analysis of **DSi20**: $M_n = 8.8 \text{ kg mol}^{-1}$, $M_w = 16.39 \text{ kg mol}^{-1}$, PDI = 1.86.

Supplementary Figures



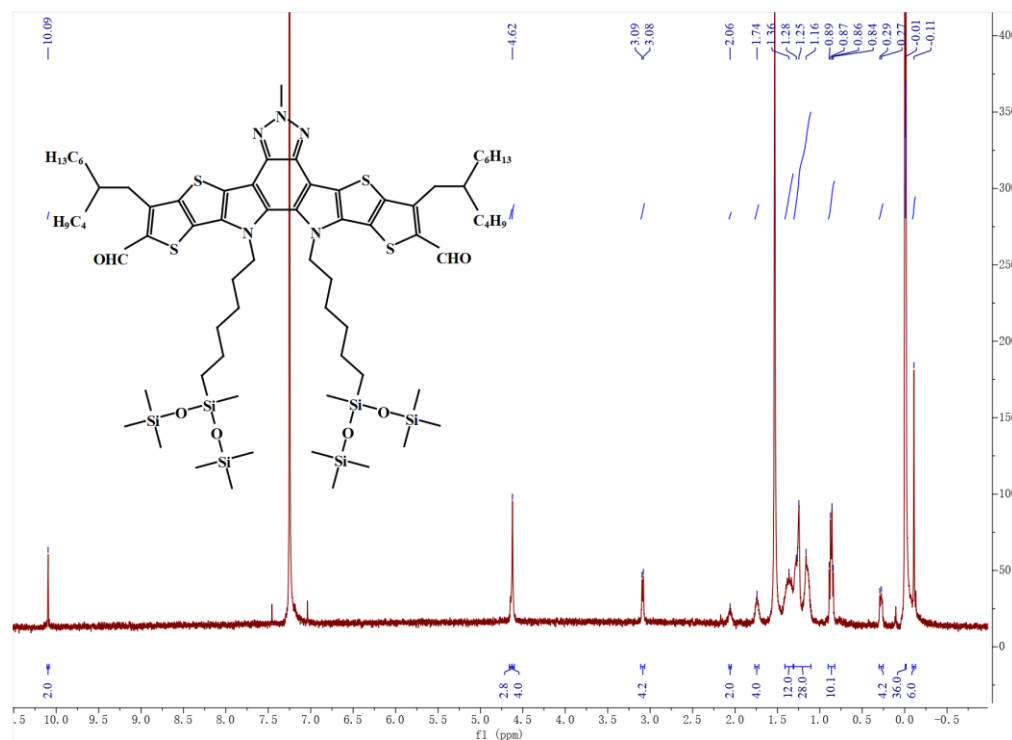


Fig. S3 ^1H NMR spectrum of Compound 4 in CDCl_3 .

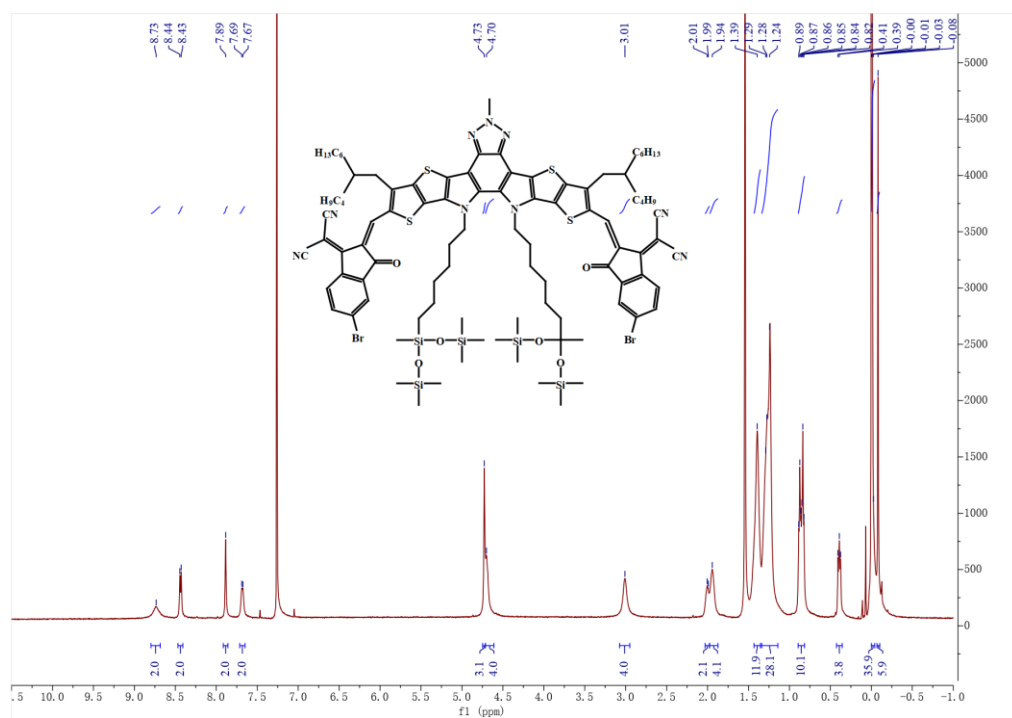


Fig. S4 ^1H NMR spectrum of BTz-C1-Si-Br in CDCl_3 .

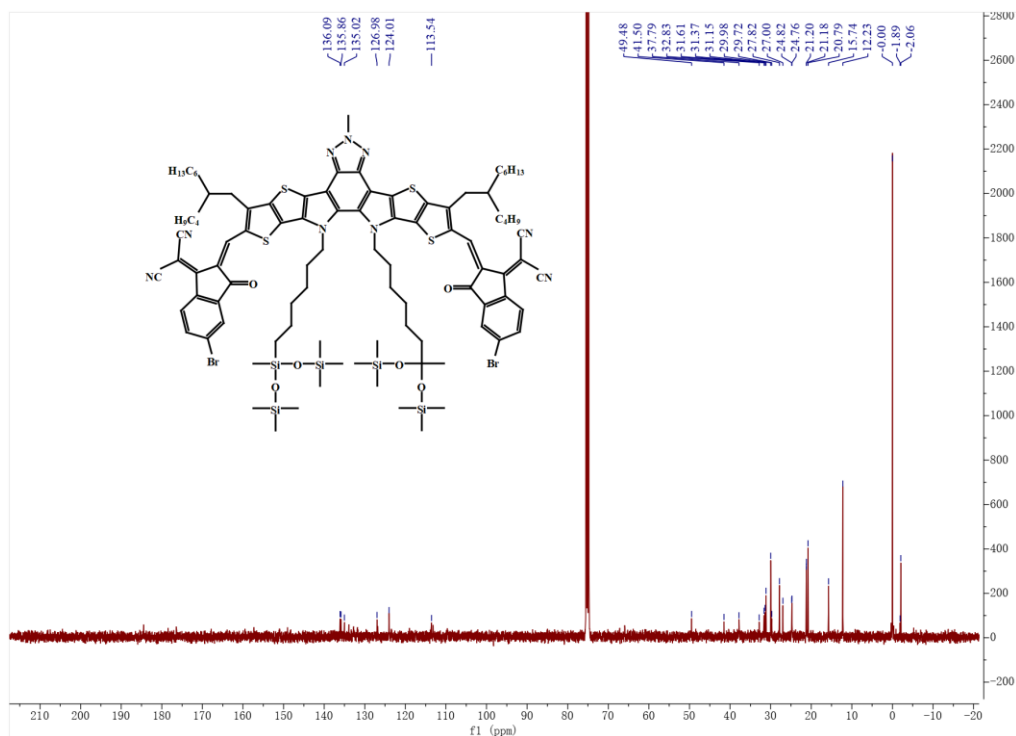


Fig. S5 ^{13}C NMR spectrum of BTz-C1-Si-Br in CDCl_3 .

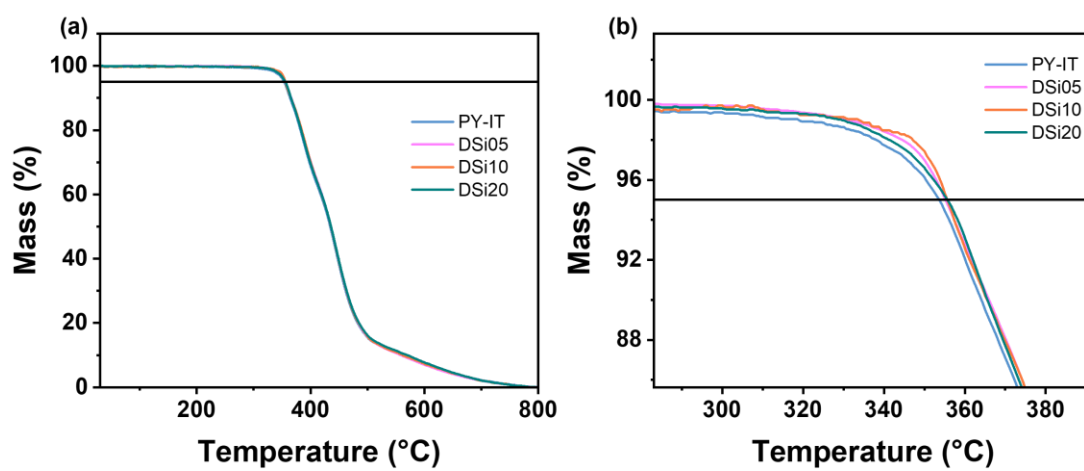


Fig. S6 (a) TGA curves of DSi series polymer acceptors and (b) their partial enlargements.

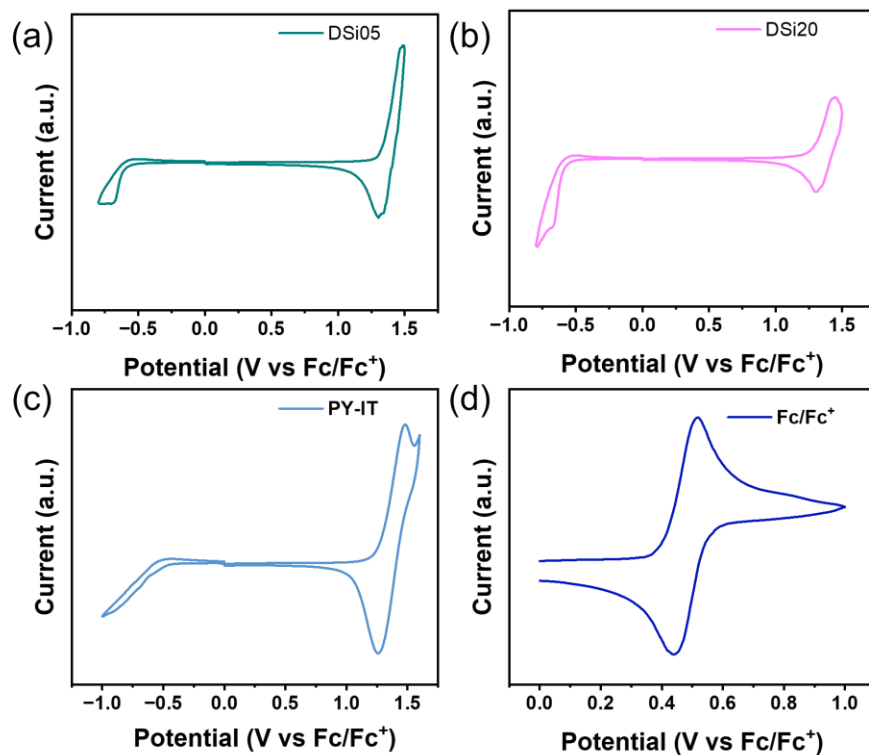


Fig. S7 CV curves of (a) DSi05, (b) DSi20, (c) PY-IT, and (d) ferrocene reference.

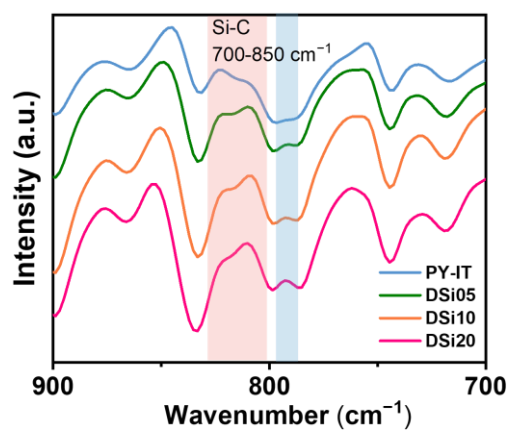


Fig. S8 Fourier transform infrared (FT-IR) spectra of bulk PY-IT and DSiX (X=05, 10, 20).

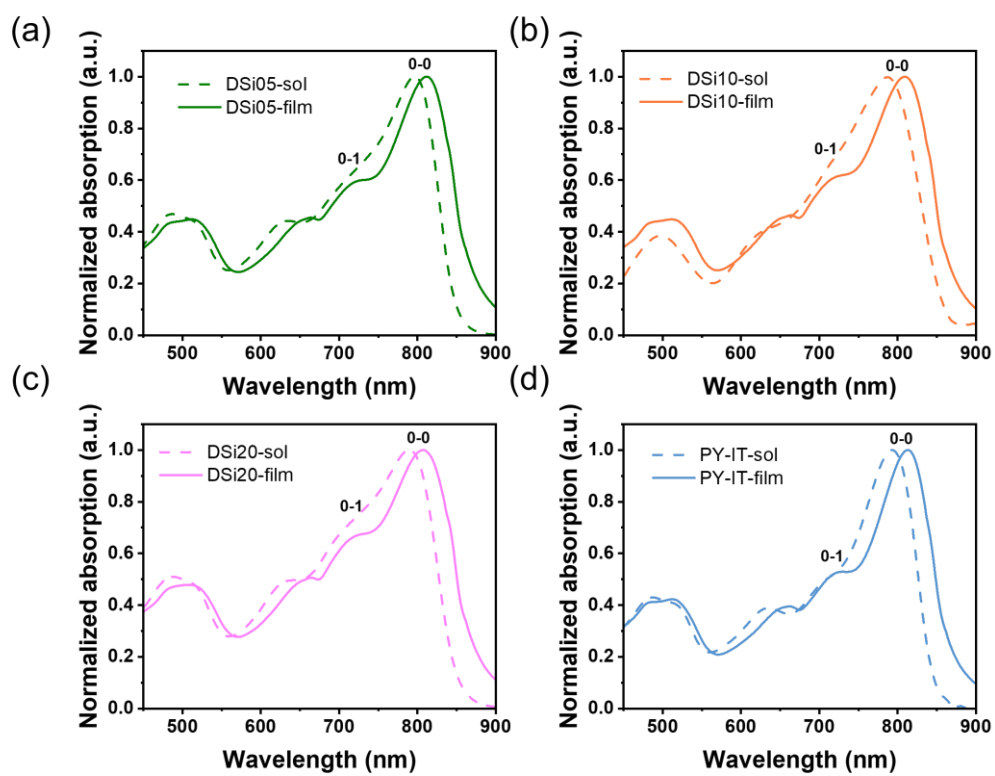


Fig. S9 Normalized UV-vis absorption spectra of solutions and films of (a) DSi05, (b) DSi10, (c) DSi20, and (d) PY-IT.

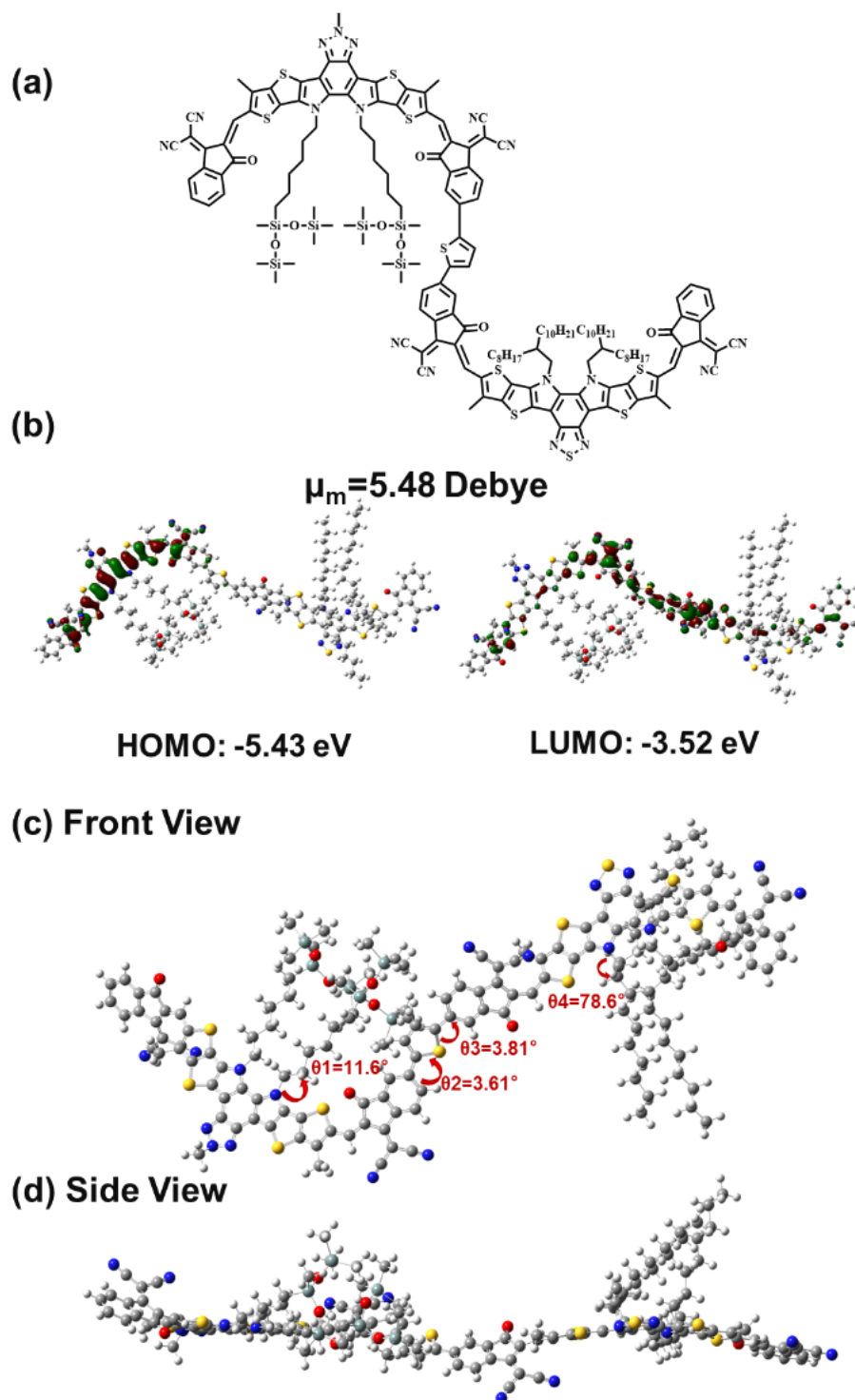


Fig. S10 (a) The skeleton of DSiX for DFT simulations where alkyl chains on thieno[3,2-b]thiophene are simplified to methyl groups. (b) Calculated molecular energy levels at the B3LYP/6-31G(d,p) level. Dihedral angle analysis of key linkages: (c) front view and (d) side view.

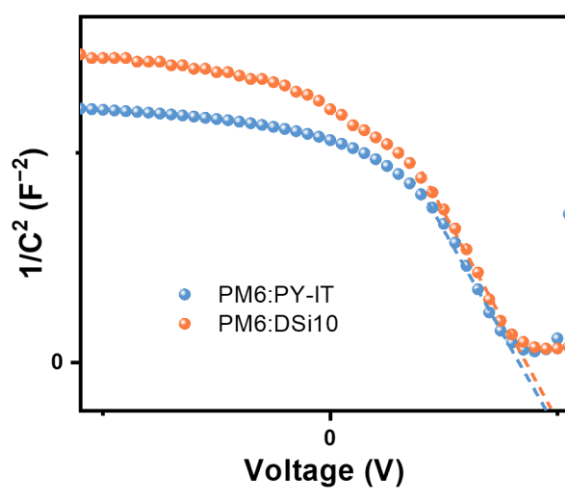


Fig. S11 Mott-Schottky analysis plots of PM6:PY-IT and PM6:DSi10 based devices

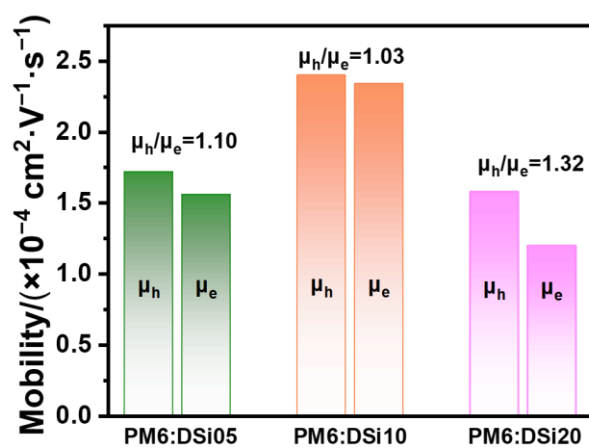


Fig. S12 Hole and electron mobilities together with the ratios of the corresponding devices.

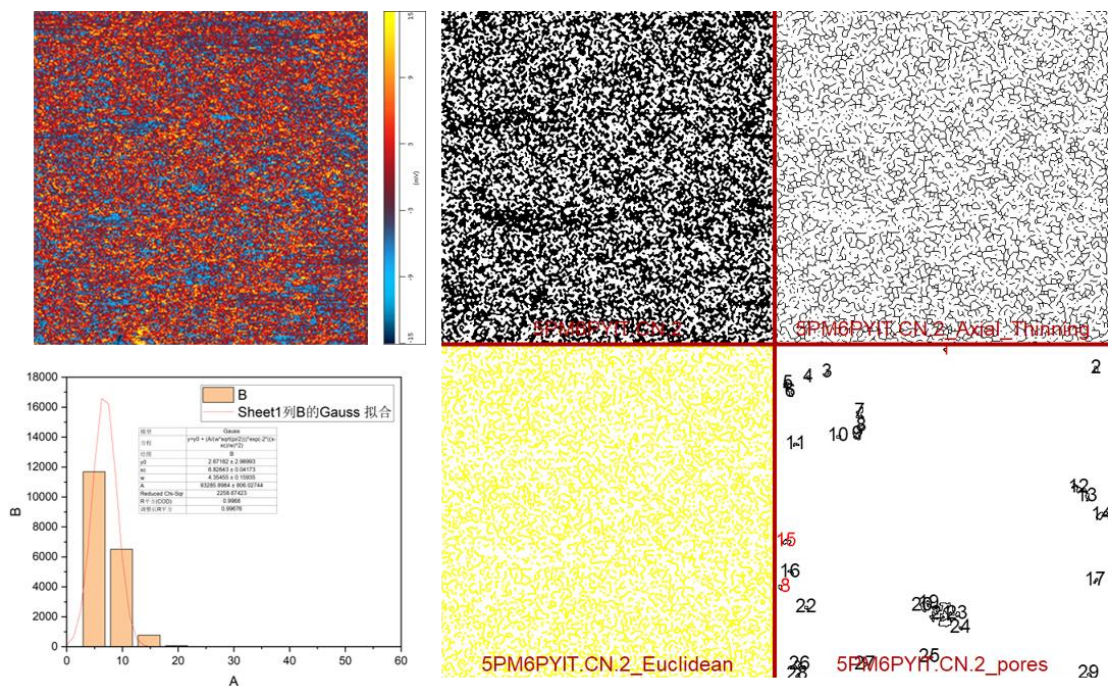


Fig. S15 The analysis of the AFM-IR phase image for PM6:PY-IT with DiameterJ software to extract the characteristic morphology and construct the model that would allow for the derivation of parameters such as fibril width and fibril density.

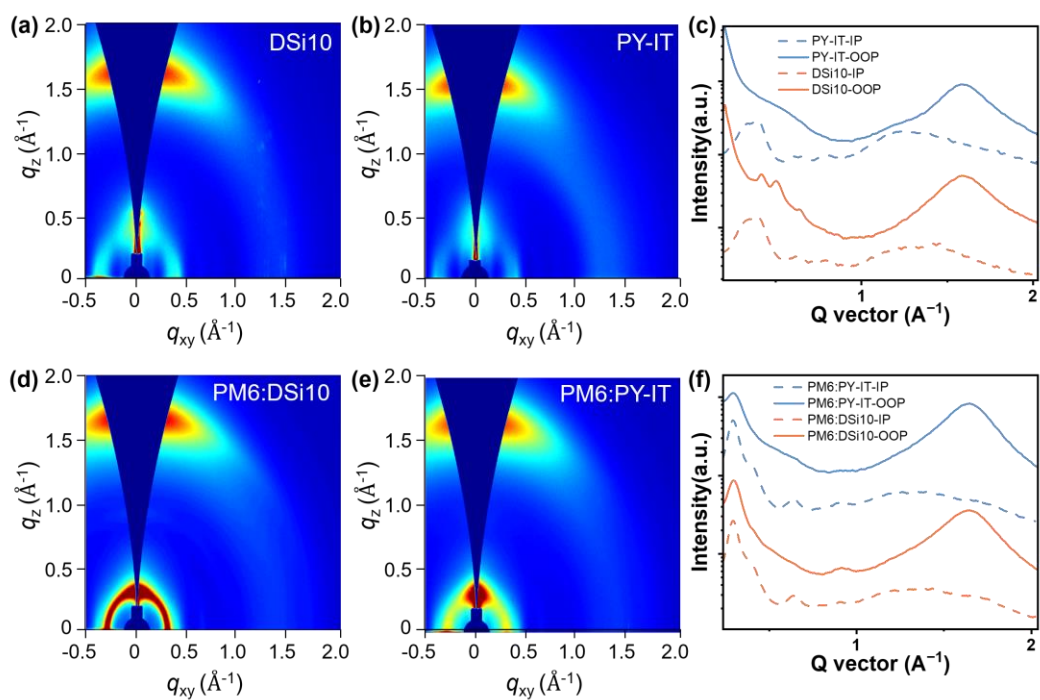


Fig. S16 2D GIWAXS patterns of (a) pure DSi10 film, (b) pure PY-IT film, (d) PM6:DSi10 blend film and (e) PM6:PY-IT blend film. (c) IP and (f) OOP profiles for

the corresponding films.

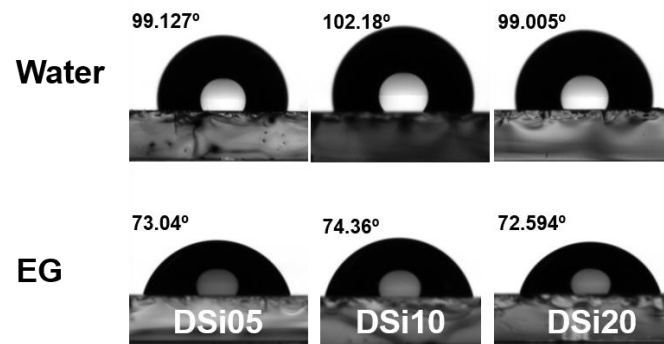


Fig. S17 Contact angles of water (H₂O) and ethylene glycol (EG) on pristine films of DSi05, DSi10, and DSi20, respectively.

Supplementary Tables

Table S1. Basic properties of DSi Series polymer acceptors.

Polymer	M_n (kDa)	M_w (kDa)	PDI
DSi05 (5%Si)	9.1	17.37	1.89
DSi10 (10%Si)	8.7	16.90	1.93
DSi20 (20%Si)	8.8	16.39	1.86

Table S2. Optical and electrochemical properties of PY-IT and DSi-series polymer acceptors.

	$\lambda_{\max}^{\text{sol}}$ (nm)	$\lambda_{\max}^{\text{film}}$ (nm)	$\lambda_{\text{onset}}^{\text{film}}$ (nm)	E_g^{opt} (eV)	E_{ox} (eV)	E_{red} (eV)	E_{HOMO}^a (eV)	E_{LUMO} (eV)
PY-IT	794	813	915	1.355	1.27	-0.56	-5.65	-3.87
DSi05	798	811	905	1.370	1.31	-0.61	-5.69	-3.82
DSi10	790	809	920	1.347	1.28	-0.61	-5.66	-3.82
DSi20	790	807	918	1.350	1.28	-0.59	-5.66	-3.84

^a $E_{\text{HOMO}} = -(E_{\text{ox}} - E_{(\text{Fc}/\text{Fc}^+)}) + 4.8$ (eV) , and $E_{(\text{Fc}/\text{Fc}^+)}$ was determined electrochemically using the ferrocene/ferrocenium (Fc/Fc⁺) couple as the internal standard. ^b $E_{\text{LUMO}} = -(E_{\text{red}} - E_{(\text{Fc}/\text{Fc}^+)}) + 4.8$ (eV) . ^d Optical band gap derived from absorption onset of the as-cast film: $E_g^{\text{opt}} = 1240 / \lambda_{\text{onset}}$.

Table S3. Peak 0–0 and 0–1 fitting parameters for the normalized UV-vis absorption spectra of PY-IT and DSi10 films.

Film	λ_{0-0}	λ_{0-1}	I_{0-1}/I_{0-0}
PY-IT	813.15	730.18	0.44
DSi10	811.17	724.58	0.53

Table S4. Photovoltaic performance parameters of all-PSCs based on PM6:DSiX (annealing at 100 °C, 10 min) under illumination of AM 1.5G, 100 mW cm⁻².

	V_{oc} (V)	J_{sc} (mA cm⁻²)	FF (%)	PCE (%)
PM6:DSi05	0.94 (0.93±0.01)	24.23 (24.05±0.201)	71.1 (70.671±0.620)	16.04 (15.82±0.350)
PM6:DSi10	0.94 (0.94±0.01)	25.23 (25.19±0.103)	73.45 (73.26±0.546)	17.37 (17.14±0.296)
PM6:DSi20	0.94 (0.93±0.01)	23.04 (22.86±0.252)	70.6 (69.72±0.922)	15.09 (14.76±0.338)

Table S5. J_{ph} at short-circuit condition, J_{sat} and P_c parameters of all-PSCs based on PM6:DSi10 and PM6:PY-IT.

Device	J_{sat} (mA cm ⁻²)	J_{ph}^a (mA cm ⁻²)	P_{diss} (%)	J_{ph}^b (mA cm ⁻²)	P_{coll} (%)
PM6:PY-IT	26.30	24.74	94.07	20.65	78.52
PM6:DSi10	26.80	25.52	95.22	21.82	81.42

^a J_{ph} at short-circuit condition; ^b J_{ph} at maximum output power.

Table S6. The hole, electron mobilities of PM6:DSi10, PM6:PY-IT-based devices obtained from SCLC measurements.

Device	μ_h (cm ² V ⁻¹ s ⁻¹)	μ_e (cm ² V ⁻¹ s ⁻¹)	μ_h/μ_e
PM6:PY-IT	1.63×10^{-4}	1.28×10^{-4}	1.27
PM6:DSi10	2.40×10^{-4}	2.34×10^{-4}	1.03

Table S7. The characteristic parameters derived from AFM-IR analysis.

Blend	Mean Fibril Width (nm)	Integrated Density
PM6:PY-IT	13.7	134.21
PM6:DSi10	24.5	118.89

Table S8. The lamellar distances (q_{xy} profile, 100) and (q_z profile, 010) of the neat polymer films and blend films.

Films	In plane			Out of plane		
	Peak Location (\AA^{-1})	d -Spacing (\AA)	CCL (\AA)	Peak Location (\AA^{-1})	d -Spacing (\AA)	CCL (\AA)
PY-IT	0.352	17.8	34.1	1.590	4.0	22.8
DSi10	0.347	18.1	37.7	1.594	3.9	23.2
PM6:PY-IT	0.294	21.4	95.9	1.632	3.8	19.6
PM6:DSi10	0.295	21.3	109.4	1.631	3.9	20.8

Table S9. Contact angle of water and ethylene glycol and the surface tension of PM6, PY-IT, and DSiX.

Film	θ_{water} ($^{\circ}$)	θ_{glycol} ($^{\circ}$)	γ^d (mJ/m 2)	γ^p (mJ/m 2)	γ (mJ/m 2)	$(\sqrt{\gamma_D} - \sqrt{\gamma_A})^2$
PM6	104.50	74.076	16.378	1.380	17.759	
PY-IT	102.09	71.476	17.169	1.743	18.913	0.018
DSi05	99.127	73.04	15.096	3.057	18.152	0.002
DSi10	102.18	74.36	15.367	2.127	17.494	0.001
DSi20	99.005	72.594	15.327	3.026	18.353	0.005

Table S10. Photovoltaic performance parameters of all-PSCs based on PM6:PY-IT and PM6:DSi10 (annealing at 100°C, 10 min) under illumination of AM 1.5G, 100 mW cm⁻².

Active layer	condition	V_{OC} (V)	J_{SC} (mA cm ⁻²)	FF (%)	PCE (%)
PM6:PY-IT	N ₂	0.94 (0.94±0.01)	23.71 (23.56±0.210)	72.98 (72.87±0.956)	16.26 (16.18±0.188)
	Air, RH 65%	0.93 (0.93±0.01)	22.56 (22.29±0.274)	71.49 (71.27±0.962)	14.99 (14.86±0.345)
	Air, RH 90%	0.93 (0.93±0.01)	22.46 (22.20±0.316)	68.00 (67.56±0.900)	14.10 (14.11±0.378)
	N ₂	0.94 (0.94±0.01)	25.23 (25.19±0.103)	73.45 (73.26±0.546)	17.37 (17.14±0.296)
PM6:DSi10	Air, RH 65%	0.94 (0.93±0.01)	24.24 (24.13±0.163)	72.95 (72.754±0.68 9)	16.60 (16.36±0.302)
	Air, RH 90%	0.94 (0.93±0.01)	23.98 (23.87±0.154)	72.79 (72.58±0.643)	16.33 (16.15±0.249)
	N ₂	0.94 (0.94±0.01)	25.23 (25.19±0.103)	73.45 (73.26±0.546)	17.37 (17.14±0.296)

Table S11. Performance parameters of air-processed all-PSCs reported in the literature.

Year	RH (%)	Active layer	V_{oc} (V)	J_{sc} (mA cm ⁻²)	FF (%)	PCE (%)	Ref.
2016	90	PTB7-Th:PDI-V	0.74	15.3	64	7.3	²
2019	0	PBDB-T:N2200	0.86	11.14	63.7	6.11	
2019	10	PBDB-T:N2200	0.86	10.99	65.5	6.2	
2019	30	PBDB-T:N2200	0.86	10.92	65.9	6.19	³
2019	50	PBDB-T:N2200	0.86	11.1	64.9	6.2	
2019	80	PBDB-T:N2200	0.86	10.97	64.2	6.06	
2019	--	PPDT2FBT-A:P(NDIDEG-T)	0.66	6.43	44	1.89	⁴
2021	--	PM6:L14	0.95	21.19	73.98	14.9	⁵
2022	50	PM6:PYF-T-o	0.887	23.9	70.8	15	
2022	50	PM6:PYF-V-o	0.874	25.2	72.9	16.1	⁶
2022	50	PM6:PYF-TT-o	0.867	24	68.5	14.3	
2022	50	PM6:PYF-DT-o	0.899	22.8	67.8	13.9	
2022	--	PM6:J71:PY-IT	0.942	22.29	72.7	15.74	⁷
2025	90	PM6:DSi10	0.94	23.98	72.79	16.33	This work

Table S12. Photovoltaic performance parameters of flexible devices based on PM6:PY-IT and PM6:DSi10.

Active layer	V_{oc} (V)	J_{sc} (mA cm ⁻²)	FF (%)	PCE (%)
PM6:PY-IT	0.910	21.72	72.64	14.33
	(0.90±0.010)	(21.75±0.256)	(72.46±0.920)	(14.30±0.256)
PM6:DSi10	0.908	22.21	72.77	14.63
	(0.90±0.011)	(22.22±0.179)	(72.67±0.756)	(14.60±0.153)

References

- 1 H. Fu, Y. Li, J. Yu, Z. Wu, Q. Fan, F. Lin, H. Y. Woo, F. Gao, Z. Zhu and A. K. Y. Jen, *J. Am. Chem. Soc.*, 2021, **143**, 2665-2670.
- 2 Y. Guo, Y. Li, O. Awartani, J. Zhao, H. Han, H. Ade, D. Zhao and H. Yan, *Adv. Mater.*, 2016, **28**, 8483-8489.
- 3 S. Lee, Y. Kim, Z. Wu, C. Lee, S. J. Oh, N. T. Luan, J. Lee, D. Jeong, K. Zhang, F. Huang, T. S. Kim, H. Y. Woo and B. J. Kim, *ACS Appl Mater Interfaces*, 2019, **11**, 45038-45047.
- 4 Y. Xu, J. Yuan, S. Zhou, M. Seifrid, L. Ying, B. Li, F. Huang, G. C. Bazan and W. Ma, *Adv. Funct. Mater.*, 2019, **29**, 1806747.
- 5 B. Liu, H. Sun, J.-W. Lee, J. Yang, J. Wang, Y. Li, B. Li, M. Xu, Q. Liao, W. Zhang, D. Han, L. Niu, H. Meng, B. J. Kim and X. Guo, *Energy Environ. Sci.*, 2021, **14**, 4499-4507.
- 6 H. K. Kim, H. Yu, M. Pan, X. Shi, H. Zhao, Z. Qi, W. Liu, W. Ma, H. Yan and S. Chen, *Adv. Sci.*, 2022, **9**, 2202223.
- 7 R. Ma, K. Zhou, Y. Sun, T. Liu, Y. Kan, Y. Xiao, T. A. D. Peña, Y. Li, X. Zou, Z. Xing, Z. Luo, K. S. Wong, X. Lu, L. Ye, H. Yan and K. Gao, *Matter*, 2022, **5**, 725-734.